Robust Adaptive Path Following Controllers
for Autonomous Surface Vehicles with Unknown Disturbances

Quoc Van Tran*, Quang-Hoang Nguyen

School of Mechanical Engineering, Hanoi University of Science and Technology, Ha Noi, Vietnam
Corresponding author email: quoc.tranvan@hust.edu.vn

Abstract

This work presents robust path following controllers with disturbance rejection terms for autonomous surface vehicles in the presence of unknown bounded disturbances. The objective is to steer the vehicle to the desired path while its temporal evolution on the path is defined via a path parameter. The disturbance rejection terms are based on sliding mode control utilizing either constant or time-varying gains. To mitigate the chattering effect in the sliding mode controllers, a continuous adaptive control law based on a normalization technique is subsequently developed. Since the control protocols are proposed as control forces based on the nonlinear dynamics of the surface vehicle, Lyapunov stability theory and backstepping control technique are adopted for the control system design and the global stability analysis. Under the proposed controllers, the vehicle is shown to converge to the desired path asymptotically. Simulation results are also provided to support the theoretical analysis.

Keywords: Autonomous surface vessels, path following, robust adaptive control, sliding mode control.

1. Introduction

The development and deployment of autonomous surface vehicles (ASVs) for missions such as search and rescue, exploration of natural resources, environmental monitoring, and surveillance in ocean environments, have been of particular interest over the past decades. When performing such a task in an open sea, the surface vehicle is often asked to follow a reference path, which is specified appropriately for the task [1-5]. For example, in a formation maneuvering of multiple surface vessels [6], one or more leading vessels are required to track a predefined trajectory. The remaining vessels keep up with the leading vessels by maintaining relative positions to nearby vessels.

When the aim is to steer the vehicle to the desired path while the evolution of its position along the trajectory is not necessarily specified with time but in any other variables, such a problem is called *path following*. As a result, in path following, the vehicle is driven to the path with a small cross-track error and then travels along it at some desired speed profile, which is generally a function of the path parameter. A multitude of path following control schemes have been presented in the literature [2-8]. There are geometric control approaches based on light-of-sight (LOS) methods [3, 7-9], the constant bearing approach (CB) [11], and the vector field (VF) guidance law [10]. The LOS control approach derives a light-of-sight angle corresponding to the bearing from the surface vessel to a point, at a certain distance ahead of the nearest point,

on the tangent axis of the path. The vehicle aligns its longitudinal axis to the look-ahead direction to follow the path [9]. When constant disturbances are present, LOS control methods with integral action were investigated in [7, 8]. The CB law aligns the vehicle's forward speed to point to the target vehicle in the path, thus a two-point guidance law [11]. In the VF method, velocity vector fields are generated around the desired path, along which the vehicle follows to eventually reach the path [10]. Lee, Tran, and Kim [4, 5] utilized tube-based model predictive control (TMPC) for docking with obstacle avoidance of fully actuated surface ships.

For underactuated surface vehicles, the number of independent controls is less than the dimension of the operating space. Path following control protocols have been developed for ASVs based largely on sliding mode control and backstepping methods [2, 6, 11-13]. The study [11] explored an extended state observer-based LOS controller with an integral sliding mode control used to deal with uncertainties. A sliding mode control based on radial neural networks was presented in [12] for path following subject to disturbances and model uncertainty. Disturbance observer and artificial potential field (APF) techniques were employed in [13]. However, the aforementioned works often assume the boundedness of the non-actuated motion.

A few works have studied path following control for underactuated surface vehicles with consideration

of the stability of the non-actuated motion [2, 6]. In [2], one allows an arbitrary small deviation around the reference path to make the control input matrix in the error dynamics invertible. The control force is then designed by utilizing backstepping control and unknown model parameters are estimated by adaptive laws [2]. As an alternative, an offset point on the forward axis, ahead of the mass center, of the vehicle, called the hand point, is driven to the reference path in [6].

This work addresses path following control for autonomous surface vehicles in the presence of unknown bounded disturbances. Although the fully-actuation nature of the vehicle sounds less attractive, the current work aims to propose and compare several robust adaptive controllers for path tracking control under unknown disturbances. Compared with those [3, 7-8, 10-11] commonly designed for kinematic models (as velocity inputs), the proposed control schemes are developed as forces/torques for dynamical surface vehicles. Furthermore, to overcome the chattering effect in sliding mode controllers [1,11,12], a continuous adaptive control law is studied using a normalization method. Numerical simulations show that, among the presented controllers, the continuous adaptive controller achieves the lowest tracking error with smoother control forces. Lyapunov stability theory and backstepping control technique are adopted for the control system design, the stability analysis, and proving asymptotic convergence of the path following control.

In the conference version of this work [1], a robust path following controller based on sliding mode control with a known upper bound of disturbances was presented. Compared with [1], robust adaptive controllers are investigated to address the path following of surface vehicles when the bound of the disturbances is unknown. In these proposed controllers, adaptive gains evolving with time, instead of fixed gains [1], of the disturbance rejection control are utilized. In contrast to [1], a continuous adaptive tracking controller and several numerical simulations are presented in this work.

The rest of the paper is organized as follows. Path following control problem is stated in Section 2. Section 3 presents the path following control laws. Simulation results are given in Section 4. Finally, Section 4 concludes this paper.

We use bold lowercase letters $\mathbf{a}, \mathbf{b}, \mathbf{c}$ and bold uppercase letters $\mathbf{A}, \mathbf{B}, \mathbf{C}$ to denote vectors and matrices, respectively. The transpose of a matrix is $\mathbf{A}^\top$. The notations $\| \cdot \|_1, \| \cdot \|$, and $\| \cdot \|_\infty$ specify the 1-norm, 2-norm, and infinity norm, respectively.

2. The Vehicle's Dynamic Model and Path Following Control

2.1. Coordinate Systems and the Dynamics of the Surface Vehicle

Consider a fully actuated surface vehicle operating in an open sea whose position $\mathbf{p} = [x, y]^\top$ is measured with regard to the inertial (North-East) coordinate system $\{\mathcal{I}\}$ (see Fig. 1). The longitudinal and lateral coordinate axes of the vehicle are fixed to its center.
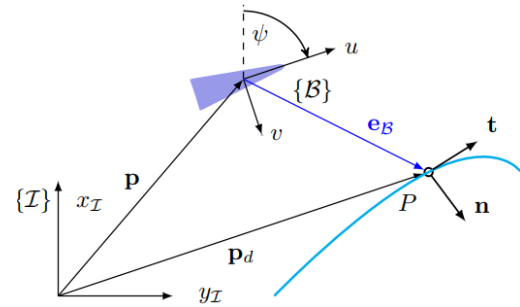

Fig. 1. Inertial coordinates, body-fixed coordinate system $\{\mathcal{B}\}$, and path coordinate system $\{\mathbf{t}, \mathbf{n}\}$.

The linear velocity of the vehicle expressed in $\{\mathcal{B}\}$ is $\mathbf{v} = [u, v]^\top$, which contains the surge and sway speeds. The orientation angle of $\{\mathcal{B}\}$ relative to $\{\mathcal{I}\}$ measured clockwise is ψ and the angular rate $r = \dot{\psi}$. The kinematic relationships between the local and inertial components of the vehicle's velocity are

$$\dot{x} = u\cos(\psi) - v\sin(\psi),$$
$$\dot{y} = u\sin(\psi) + v\cos(\psi), \qquad \dot{\psi} = r. \tag{1}$$

Denote the rotation matrix

$$\mathbf{R}(\psi) = \begin{bmatrix} \cos\psi & -\sin\psi \\ \sin\psi & \cos\psi \end{bmatrix} \in SO(2).$$

Thus, $\dot{\mathbf{p}} = \mathbf{R}\mathbf{v}$; the rotational kinematics is as

$$\dot{\mathbf{R}}(\psi) = \begin{bmatrix} \cos\psi & -\sin\psi \\ \sin\psi & \cos\psi \end{bmatrix} \begin{bmatrix} 0 & -r \\ r & 0 \end{bmatrix} := \mathbf{R}\mathbf{S}(r), \tag{2}$$

where $\mathbf{S}(r)$ is a skew-symmetric matrix. Let $v = [u, v, r]^\top$ be the vehicle's body velocity. The 3-DOF planar motion of the surface vehicle is given in the local coordinates as follows

$$\mathbf{M}\dot{v} + \mathbf{C}(v)v + \mathbf{D}v = \boldsymbol{\tau}_c + \boldsymbol{\tau}_w. \tag{3}$$

Here, $\mathbf{M}, \mathbf{C}(v)$ and $\mathbf{D} \in \mathbb{R}^{3\times3}$ denote the mass,

Coriolis, and damping matrices, respectively. $\boldsymbol{\tau}_c$ and $\boldsymbol{\tau}_w \in \mathbb{R}^3$ are the control and disturbance vectors, respectively. These dynamic matrices are given as follows [14]:

$$\mathbf{M} = \begin{bmatrix} m_{11} & 0 & 0 \\ 0 & m_{22} & m_{23} \\ 0 & m_{32} & m_{33} \end{bmatrix}, \mathbf{D} = -\begin{bmatrix} X_u & 0 & 0 \\ 0 & Y_v & Y_r \\ 0 & N_v & N_r \end{bmatrix},$$

$$\mathbf{C} = \begin{bmatrix} 0 & 0 & -m_{22}v - m_{23}r \\ 0 & 0 & m_{11}u \\ m_{22}v + m_{23}r & -m_{11}u & 0 \end{bmatrix}.$$

Here, m_{ij}'s are the vehicle inertia parameters and the parameters in the matrix $\mathbf{D}$ are the hydrodynamic damping coefficients.

For the control design purpose, the forward dynamics

$$\dot{v} = \mathbf{M}^{-1}(-\mathbf{C}(v)v - \mathbf{D}v) + \mathbf{M}^{-1}(\boldsymbol{\tau}_c + \boldsymbol{\tau}_w)$$

is written in the general nonlinear dynamics:

$$\dot{\mathbf{v}} = \mathbf{f}(v) + \mathbf{u}_c + \mathbf{w}_v, \tag{4}$$

$$\dot{r} = g(v) + u_r + w_r, \tag{5}$$

where the nonlinear functions are defined as $[\mathbf{f}^\top, g]^\top = \mathbf{M}^{-1}(-\mathbf{C}(v)v - \mathbf{D}v)$, $[\mathbf{u}_c^\top, u_r]^\top := \mathbf{M}^{-1}\boldsymbol{\tau}_c$ and $[\mathbf{w}_v^\top, w_r]^\top := \mathbf{M}^{-1}\boldsymbol{\tau}_w$.

2.2. Defining the Desired Path

The curved *path* $\mathcal{P}$ to follow by the vehicle is parameterized by $\gamma \in \Omega = [a,b]$, where the two end points of the path are defined at $\gamma = a$ and $\gamma = b \in \mathbb{R}$. The position and velocity of a point $P \in \mathcal{P}$, denoted as $\mathbf{p}_d$ and $\mathbf{v}_d$, respectively, are:

$$\mathbf{p}_d(\gamma) = [x_d(\gamma), y_d(\gamma)]^\top,$$
$$\mathbf{v}_d = \frac{d\mathbf{p}_d(\gamma)}{dt} = \frac{\partial \mathbf{p}_d}{\partial \gamma} \frac{d\gamma}{dt} = \mathbf{p}_d'(\gamma)\dot{\gamma}. \tag{6}$$

In the trajectory tracking problem, i.e., the position of the vehicle in the path is explicitly specified with time, the path parameter γ is simply the time variable t. When $\gamma = s$, the distance traveled by the vehicle, one has $\|\mathbf{p}_d'(\gamma)\| = 1$. A parallel-transport path frame is constructed at each point $P \in \mathcal{P}$ consisting of the tangent vector $\mathbf{t}$ to the path and normal vector $\mathbf{n}$ (see Fig. 1). The tangent vector is:

$$\mathbf{t}(\gamma) = \mathbf{p}_d'(\gamma) / \|\mathbf{p}_d'(\gamma)\|.$$

$\mathbf{n}$ is obtained by rotation of $\mathbf{t}$ about P $\pi/2$ radians clockwise.

2.3. Path Following Control Problem

A path following force controller (i.e., $\boldsymbol{\tau}_c$) aims at steering the surface vehicle to the desired location in the path, i.e.,

$$\mathbf{e} := (\mathbf{p}_d(\gamma) - \mathbf{p}) \to \mathbf{0}, \text{ as } t \to \infty.$$

The evolution of the vehicle along the path is determined by the path parameter $\gamma(t)$. Denote by $U_d(t) \in \mathbb{R}^+$ the desired speed of the vehicle in the path. When the path following is achieved, the desired velocity of the vehicle in $\mathcal{P}$, $\|\mathbf{v}_d\| = \|\mathbf{p}_d'(\gamma)\|\dot{\gamma}$ converges to $U_d(t)$ asymptotically. Consequently, the tracking error of the parameter's speed is obtained by

$$e_\gamma = \dot{\gamma} - U_d / \|\mathbf{p}_d'(\gamma)\| := \dot{\gamma} - v_d. \tag{7}$$

Here v_d is the desired speed of γ. Define the position error in the local coordinates (see Fig. 1):

$$\mathbf{e}_\mathcal{B} = \mathbf{R}^\top(\psi)(\mathbf{p}_d - \mathbf{p}). \tag{8}$$

The derivative of $\mathbf{e}_\mathcal{B}$ can be shown to be:

$$\dot{\mathbf{e}}_\mathcal{B} = -\mathbf{S}(r)\mathbf{e}_\mathcal{B} - \mathbf{v} + \mathbf{R}^\top(\psi)\mathbf{p}_d'(\gamma)\dot{\gamma}. \tag{9}$$

By (7) and (9), the error dynamics of the control system with the state $\mathbf{x} = [\mathbf{e}_\mathcal{B}^\top, e_\gamma]^\top \in \mathbb{R}^3$ is:

$$\dot{\mathbf{x}} = \begin{bmatrix} -\mathbf{S}(r)\mathbf{e}_\mathcal{B} - \mathbf{v} + \mathbf{R}^\top(\psi)\mathbf{p}_d'(\gamma)\dot{\gamma} \\ \ddot{\gamma} - \dot{v}_d \end{bmatrix}. \tag{10}$$

3. Robust Path Following Control Protocols

Path following control schemes are proposed for the surface vehicle when the bound of the disturbances is either known or unknown. To this end, we design the *reference velocity* $\mathbf{v}_{ref}$ (or i.e., kinematic guidance law) and the path parameter's second derivative $\ddot{\gamma}$ as follows

$$\mathbf{v}_{ref} = \mathbf{K}_p \mathbf{e}_\mathcal{B} + \mathbf{R}^\top(\psi)\mathbf{p}_d'(\gamma)v_d,$$
$$\ddot{\gamma} = -k_\gamma e_\gamma + \dot{v}_d - \mathbf{e}_\mathcal{B}^\top \mathbf{R}^\top(\psi)\mathbf{p}_d'(\gamma). \tag{11}$$

Here, $k_\gamma > 0$ and $\mathbf{K}_p \in \mathbb{R}^{2\times 2}$ is a positive definite matrix. It is desired to drive $\mathbf{v}$ to track the reference velocity $\mathbf{v}_{ref}$, for $\mathbf{v} \equiv \mathbf{v}_{ref}$ in (10) the path following can be shown to be achieved. The rotational degree of freedom (5) can utilized to stabilize $\psi = \psi_d$ for a desired yaw profile $\psi_d(t)$. For example, if the tangent to the path were chosen, one would have $\psi_d(t) = \text{atan2}(y_d', x_d')$. To proceed, the velocity error vector $\mathbf{z}$ and its time derivative are respectively defined by

$$\mathbf{z} := \mathbf{v} - \mathbf{v}_{ref} = \mathbf{v} - \mathbf{K}_p \mathbf{e}_\mathcal{B} - \mathbf{R}^\top(\psi)\mathbf{p}_d'(\gamma)\nu_d,$$

$$\dot{\mathbf{z}} = \mathbf{f}(\nu) + \mathbf{u}_c + \mathbf{w}_\mathbf{v} - \mathbf{K}_p \dot{\mathbf{e}}_\mathcal{B} + \mathbf{S}(r)\mathbf{R}^\top(\psi)\mathbf{p}_d'(\gamma)\nu_d$$
$$-\mathbf{R}^\top(\psi)\mathbf{p}_d''(\gamma)\nu_d\dot{\gamma} - \mathbf{R}^\top(\psi)\mathbf{p}_d'(\gamma)\dot{\nu}_d. \tag{12}$$

3.1. Path Following Control with a Known Upper Bound of the Disturbances

The control design is based on a backstepping technique. We propose the following control law [1]:

$$\mathbf{u}_c = -k_z \mathbf{z} - \mathbf{f}(\nu) - \beta \mathrm{sign}(\mathbf{z}) + \mathbf{K}_p \dot{\mathbf{e}}_\mathcal{B}$$
$$-\mathbf{S}(r)\mathbf{R}^\top(\psi)\mathbf{p}_d'(\gamma)\nu_d + \mathbf{R}^\top(\psi)\mathbf{p}_d'(\gamma)\dot{\nu}_d$$
$$+\mathbf{R}^\top(\psi)\mathbf{p}_d''(\gamma)\nu_d\dot{\gamma}. \tag{13}$$

Here, $\dot{\mathbf{e}}_\mathcal{B}$ is given in (9), the control gain is greater than the bound of the disturbance $\beta > \|\mathbf{w}_\mathbf{v}\|_\infty$, and $\mathrm{sign}(\cdot)$ is the component-wise signum function. We can now prove the following theorem, which has also been stated in [1].

Theorem 1: Consider the vessel's dynamics (3) and path-following error dynamics (10). Suppose that the desired path $\mathbf{p}_d(\gamma)$ is twice differentiable with respect to γ and $k_z > 1/(4\lambda_{\min}(\mathbf{K}_p))$. Then, under the controller (13), the path-following error $\mathbf{x} \to \mathbf{0}$ asymptotically as time diverges.

Proof: First, the choice of $\mathbf{v} = \mathbf{v}_{ref}$ and $\dot{\gamma}$ in (11) ensures the path following objective. This is due to the derivative of the Lyapunov function $V_1 = (1/2)\mathbf{x}^\top\mathbf{x}$ along the trajectory of (10) satisfies $\dot{V}_1 \le -\lambda_{min}\left(\mathrm{diag}(\mathbf{K}_p, k_\gamma)\right)\|\mathbf{x}\|^2$ (see Lemma 1 in [1]).

In the second step, we show that under the proposed controller (13), $\mathbf{z} = \mathbf{v} - \mathbf{v}_{ref}$ can be stabilized to zero and $\mathbf{x} \to \mathbf{0}$ asymptotically as $t \to \infty$. We consider the Lyapunov function

$$V = (1/2)\mathbf{x}^\top\mathbf{x} + (1/2)\mathbf{z}^\top\mathbf{z},$$

which is positive definite, continuously differentiable, and radially unbounded. Since (13) is nonsmooth, the differential inclusion operation $\mathcal{K}(\cdot)$ is used to compute $\dot{V}$ [15]. In particular, by (10), (12), and the skew-symmetry property of $\mathbf{S}(r)$, i.e., $\mathbf{e}_\mathcal{B}^\top\mathbf{S}(r)\mathbf{e}_\mathcal{B} = 0$ for any vector $\mathbf{e}_\mathcal{B}$, one has

$$\dot{V} = -\mathbf{e}_\mathcal{B}^\top\mathbf{K}_p\mathbf{e}_\mathcal{B} - k_\gamma e_\gamma^2 - \mathbf{e}_\mathcal{B}^\top\mathbf{z} - k_z\|\mathbf{z}\|^2$$
$$-\beta\mathbf{z}^\top\mathrm{sign}(\mathbf{z}) + \mathbf{z}^\top\mathbf{w}_\mathbf{v}$$
$$\le -\lambda_{\min}(\mathbf{K}_p)\mathbf{e}_\mathcal{B}^\top\mathbf{e}_\mathcal{B} - k_\gamma e_\gamma^2 - \mathbf{e}_\mathcal{B}^\top\mathbf{z} - k_z\|\mathbf{z}\|^2$$
$$-\left(\beta - \|\mathbf{w}_\mathbf{v}\|_\infty\right)\|\mathbf{z}\|_1$$
$$\le -\lambda_{\min}\left(\mathbf{e}_\mathcal{B} + \frac{\mathbf{z}}{2\lambda_{\min}}\right)^2 - k_\gamma e_\gamma^2 - \left(k_z - \frac{1}{4\lambda_{\min}}\right)\|\mathbf{z}\|^2,$$

where, in the first inequality we have used $z^\top\mathcal{K}(\mathrm{sign}(\mathbf{z})) = z^\top\mathrm{sign}(\mathbf{z}) = \|\mathbf{z}\|_1$ and $\mathbf{z}^\top\mathbf{w}_\mathbf{v} \le \|\mathbf{z}\|_1\|\mathbf{w}_\mathbf{v}\|_\infty$. It follows that when $k_z > 1/(4\lambda_{\min})$,

$\dot{V} \le 0$ and hence $V(t)$ is uniformly bounded. As a result, $\|\mathbf{e}_\mathcal{B}\|, \|e_\gamma\|$, and $\|\mathbf{z}\|$ are bounded. By (9), (11) and (12), $\ddot{\gamma}$, $\dot{\mathbf{e}}_\mathcal{B}$, and $\dot{\mathbf{z}}$ are uniformly bounded. Therefore, it can be shown that $\ddot{V}$ is bounded and thus $\dot{V}$ is uniformly continuous. By Barbalat's lemma, $\dot{V} \to 0$ as $t \to \infty$. As a consequence, $\mathbf{x} \to \mathbf{0}$ and $\mathbf{z} \to \mathbf{0}$ asymptotically as $t \to \infty$ and the Theorem is proven.

3.2. Robust Adaptive Path Following Control with Unknown Disturbances

When the bound of the disturbances $\|\mathbf{w}_\mathbf{v}\|_\infty$ is unknown, we propose the following controller with an adaptive gain $\hat{\beta}$:

$$\mathbf{u}_c = -k_z\mathbf{z} - \mathbf{f}(\nu) - \hat{\beta}(t)\mathrm{sign}(\mathbf{z}) + \mathbf{K}_p\dot{\mathbf{e}}_\mathcal{B}$$
$$-\mathbf{S}(r)\mathbf{R}^\top(\psi)\mathbf{p}_d'(\gamma)\nu_d + \mathbf{R}^\top(\psi)\mathbf{p}_d'(\gamma)\dot{\nu}_d$$
$$+\mathbf{R}^\top(\psi)\mathbf{p}_d''(\gamma)\nu_d\dot{\gamma}. \tag{14}$$

$$\dot{\hat{\beta}}(t) = k_\beta\|\mathbf{z}\|_1, \quad \hat{\beta}(0) > 0. \tag{15}$$

Here, $k_\beta > 0$ is the update rate of the adaptive gain $\hat{\beta}$. The use of a "*leaky*" integration (15) helps to adjust the gain $\hat{\beta}$ until it equals or exceeds $\|\mathbf{w}_\mathbf{v}\|_\infty$ so as to make the derivative of a Lyapunov candidate function negative [16]. We can now prove an asymptotic convergence of the path following as follows.

Theorem 2: Consider the vessel's dynamics (3) and path-following error dynamics (10). Suppose that the desired path $\mathbf{p}_d(\gamma)$ is twice differentiable with respect to γ and $k_z > 1/(4\lambda_{\min}(\mathbf{K}_p))$. Then, under the adaptive controller (14)-(15), the path-following error $\mathbf{x} \to \mathbf{0}$ asymptotically as $t \to \infty$.

Proof: Consider the derivative of the Lyapunov function

$$V_1 = (1/2)\mathbf{x}^\top\mathbf{x} + (1/2)\mathbf{z}^\top\mathbf{z} + (\hat{\beta} - \beta_{\max})^2/(2k_\beta).$$

Here $\beta_{\max} > \|\mathbf{w}_\mathbf{v}\|_\infty$ is an arbitrary gain that is used only for the analysis. The derivative of V along the trajectory of (10) is given by

$$\dot{V}_1 = -\mathbf{e}_\mathcal{B}^\top\mathbf{K}_p\mathbf{e}_\mathcal{B} - k_\gamma e_\gamma^2 - \mathbf{e}_\mathcal{B}^\top\mathbf{z} - k_z\|\mathbf{z}\|^2$$
$$+(\hat{\beta} - \beta_{\max})\|\mathbf{z}\|_1 - \hat{\beta}\mathbf{z}^\top\mathrm{sign}(\mathbf{z}) + \mathbf{z}^\top\mathbf{w}_\mathbf{v}$$
$$\le -\lambda_{\min}(\mathbf{K}_p)\mathbf{e}_\mathcal{B}^\top\mathbf{e}_\mathcal{B} - k_\gamma e_\gamma^2 - \mathbf{e}_\mathcal{B}^\top\mathbf{z} - k_z\|\mathbf{z}\|^2$$
$$+(\hat{\beta} - \beta_{\max})\|\mathbf{z}\|_1 - \hat{\beta}\|\mathbf{z}\|_1 + \|\mathbf{w}_\mathbf{v}\|_\infty\|\mathbf{z}\|_1$$
$$\le -\lambda_{\min}(\mathbf{K}_p)\mathbf{e}_\mathcal{B}^\top\mathbf{e}_\mathcal{B} - k_\gamma e_\gamma^2 - \mathbf{e}_\mathcal{B}^\top\mathbf{z} - k_z\|\mathbf{z}\|^2$$
$$-\left(\beta_{\max} - \|\mathbf{w}_\mathbf{v}\|_\infty\right)\|\mathbf{z}\|_1.$$

The remainder of the proof follows from a similar argument as Proof of Theorem 1, thus omitted.

The control laws (13) and (14) are nonsmooth due to the use of the signum function, thus causing chattering effect. To overcome the discontinuity issue, the following control protocol is proposed using a normalization technique [16]:

$$\mathbf{u}_c = -k_z \mathbf{z} - \mathbf{f}(\nu) - \hat{\beta}(t)\frac{\mathbf{z}}{\|\mathbf{z}\| + \mu(t)} + \mathbf{K}_p \dot{\mathbf{e}}_{\mathcal{B}}$$
$$-\mathbf{S}(r)\mathbf{R}^\top(\psi)\mathbf{p}'_d(\gamma)v_d + \mathbf{R}^\top(\psi)\mathbf{p}'_d(\gamma)\dot{v}_d$$
$$+\mathbf{R}^\top(\psi)\mathbf{p}''_d(\gamma)v_d\dot{\gamma}. \qquad (16)$$

$$\dot{\hat{\beta}}(t) = k_\beta \|\mathbf{z}\|^2 / (\|\mathbf{z}\| + \mu(t)), \hat{\beta}(0) > 0. \qquad (17)$$

Here the normalizing signal is $m \triangleq \|z\| + \mu(t)$ has been used with $\mu(t) > 0$, $\forall t$, and $\int_{t=0}^{\infty} \mu(\tau)d\tau < \infty$ (e.g., $\mu(t) = e^{-at}, a > 0$).

Theorem 3: Consider the vessel's dynamics (3) and path-following error dynamics (10). Suppose that the desired path $\mathbf{p}_d(\gamma)$ is twice differentiable with respect to γ and $k_z > 1/(4\lambda_{\min}(\mathbf{K}_p))$. Then, under the adaptive controller (16)-(17), the path-following error $\mathbf{x} \to \mathbf{0}$ asymptotically as $t \to \infty$.

Proof: Using the same Lyapunov function V_1 as before, one has the derivative of V_1 along the trajectory of (10), (16), and (17) as

$$\dot{V}_1 = -\mathbf{e}_{\mathcal{B}}^\top \mathbf{K}_p \mathbf{e}_{\mathcal{B}} - k_\gamma e_\gamma^2 - \mathbf{e}_{\mathcal{B}}^\top \mathbf{z} - k_z \|\mathbf{z}\|^2$$
$$+(\hat{\beta} - \beta_{\max})\frac{\|\mathbf{z}\|^2}{\|\mathbf{z}\| + \mu(t)} - \hat{\beta}\frac{\mathbf{z}^\top \mathbf{z}}{\|\mathbf{z}\| + \mu(t)} + \mathbf{z}^\top \mathbf{w_v}$$

$$\leq -\lambda_{\min}(\mathbf{K}_p)\mathbf{e}_{\mathcal{B}}^\top \mathbf{e}_{\mathcal{B}} - k_\gamma e_\gamma^2 - \mathbf{e}_{\mathcal{B}}^\top \mathbf{z} - k_z \|\mathbf{z}\|^2$$
$$-\beta_{\max}\|\mathbf{z}\|^2 / (\|\mathbf{z}\| + \mu(t)) + \|\mathbf{w_v}\| \|\mathbf{z}\|$$

$$\leq -\lambda_{\min}(\mathbf{K}_p)\mathbf{e}_{\mathcal{B}}^\top \mathbf{e}_{\mathcal{B}} - k_\gamma e_\gamma^2 - \mathbf{e}_{\mathcal{B}}^\top \mathbf{z} - k_z \|\mathbf{z}\|^2$$
$$-\beta_{\max}\|\mathbf{z}\|^2 / (\|\mathbf{z}\| + \mu(t)) + \beta_{\max}\|\mathbf{z}\|$$

$$\leq -\lambda_{\min}(\mathbf{K}_p)\mathbf{e}_{\mathcal{B}}^\top \mathbf{e}_{\mathcal{B}} - k_\gamma e_\gamma^2 - \mathbf{e}_{\mathcal{B}}^\top \mathbf{z} - k_z \|\mathbf{z}\|^2$$
$$+\beta_{\max}\mu(t)\|\mathbf{z}\| / (\|\mathbf{z}\| + \mu(t))$$

$$\leq -\lambda_{\min}(\mathbf{K}_p)\mathbf{e}_{\mathcal{B}}^\top \mathbf{e}_{\mathcal{B}} - k_\gamma e_\gamma^2 - \mathbf{e}_{\mathcal{B}}^\top \mathbf{z} - k_z \|\mathbf{z}\|^2 + \beta_{\max}\mu(t)$$

$$\leq -\lambda_{\min}\left(\mathbf{e}_{\mathcal{B}} + \frac{\mathbf{z}}{2\lambda_{\min}}\right)^2 - k_\gamma e_\gamma^2 - \left(k_z - \frac{1}{4\lambda_{\min}}\right)\|\mathbf{z}\|^2$$
$$+\beta_{\max}\mu(t),$$

where, the first inequality makes use of $\mathbf{z}^\top \mathbf{w_v} \leq \|\mathbf{w_v}\| \|\mathbf{z}\|$ and for any $\beta_{\max} > \sup_{t>0} \|\mathbf{w_v}\|$.

Consequently, $\quad 0 < V_1(t) + \lambda_{\min}\int_{t=0}^{\infty}(\mathbf{e}_{\mathcal{B}} + \frac{\mathbf{z}}{2\lambda_{\min}})^2 d\tau$

$+k_\gamma\int_{t=0}^{\infty}e_\gamma^2 d\tau + (k_z - 1/(4\lambda_{\min}))\int_{t=0}^{\infty}\|\mathbf{z}(\tau)\|^2 d\tau$

$\leq V_1(0) + \beta_{\max}\int_{t=0}^{\infty}\mu(\tau)d\tau < \infty$. Therefore, $V_1(t)$, $\mathbf{e}_{\mathcal{B}}$, e_γ and $\mathbf{z} \in \mathcal{L}_\infty$ (or i.e., uniformly bounded) and $\mathbf{e}_{\mathcal{B}}, e_\gamma, \mathbf{z} \in \mathcal{L}_2$ ($\alpha(t) \in \mathcal{L}_2$ if $\int_{t=0}^{\infty}\|\alpha(\tau)\|^2 d\tau < \infty$). By (9), (11) and (12), one has $\dot{\gamma}$, $\dot{\mathbf{e}}_{\mathcal{B}}$, and $\dot{\mathbf{z}}$ are uniformly bounded. It follows that $\mathbf{x} \to \mathbf{0}$ and $\mathbf{z} \to \mathbf{0}$ asymptotically as $t \to \infty$ according to Barbalat's lemma [16, Lem 3.2.5]. This completes the proof.

4. Simulation

For the simulations, the inertial and damping parameters of a supply ship are chosen. In particular, $m_{11} = 4.5096 \cdot 10^6$ kg, $m_{22} = 7.5608 \cdot 10^6$ kg, $m_{23} = m_{32} = -2.2680 \cdot 10^6$ kgm, $m_{33} = 2.9683 \cdot 10^7$ kgm^2, $X_u = -5.1380 \cdot 10^4$ Ns/m, $Y_v = -1.6980 \cdot 10^5$ Ns/m, $Y_r = 1.5081 \cdot 10^6$ Ns, $N_v = 1.5081 \cdot 10^6$ Ns, and $N_r = -2.5300 \cdot 10^6$ Nms. The initial position of the vehicle is $\mathbf{p}_0 = [15, -15]^\top$ (m) and the initial yaw angle $\psi_0 = \pi/3$ (rad). The control gains $k_z = 0.1$, $k_\gamma = 0.5$, and $\mathbf{K}_p = \text{diag}\{0.2, 0.1\}$ are selected for all simulation scenarios in the below. The desired path to follow $\mathbf{p}_d = [150\cos(0.5\gamma), 150\sin(0.5\gamma)]^\top$ is a circle of radius 150 (m) (the dashed blue line in Fig. 2) with the desired speed of the path parameter $v_d = 0.05$. The rotational degree of freedom is used to control the vehicle to track the tangent $\mathbf{t}(\gamma)$ to the path. Thus $\psi_d(t) = \text{atan2}(y'_d, x'_d)$ and the control input is designed as a PD-like $u_r = g(\nu) + \ddot{\psi}_d + k_\psi(\psi_d - \psi)$ for $k_\psi > 0$. The disturbance acting on the vehicle is given as $\tau_w = 10^5[\sin(0.5t), \cos(0.5t), 0]^\top$ (N). The adaptive updates (15) and (17) are implemented using the Euler's method with sampling time $T_s = 0.2$ sec.
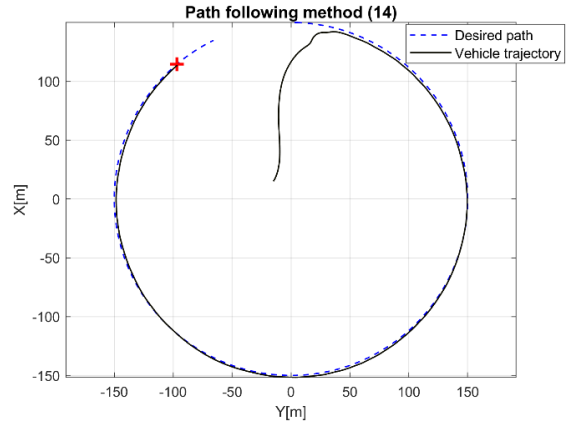
4.1. Path Following Control under Controllers (13) and (14)-(15) with the Signum Function

Simulation results for the path following control under the control law (13) with $\beta = 0$ and $\beta = 0.8$ are provided in Fig. 2(a) and 2(b), respectively.

As can be seen in Fig. 2 (a), without the sliding mode control term $\beta\text{sign}(\mathbf{z})$ in (13), the vehicle follows the path with high position error. Whereas, in the presence of $\beta\text{sign}(\mathbf{z})$ ($\beta \neq 0$), the vehicle tracks the desired path successfully. However, chattering effect occurs in the control τ_c (plotted only the surge and sway forces) due to the use of the signum function, as shown in Fig. 2(c). The yaw angle $\psi(t)$ versus time is shown in Fig. 2(d).
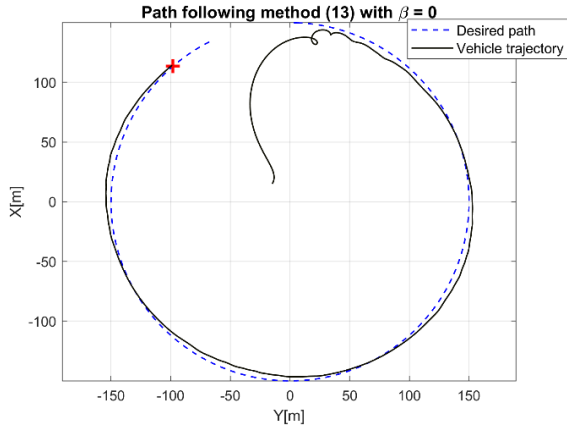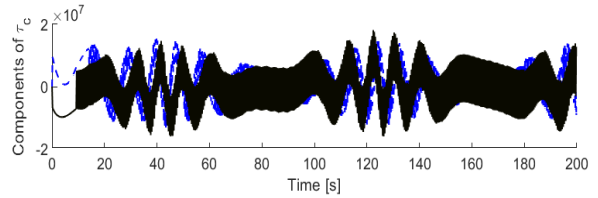
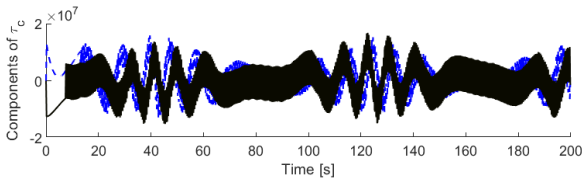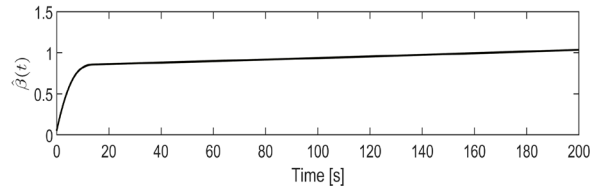a) Path tracking plotted for 250 secs.

a) Path tracking
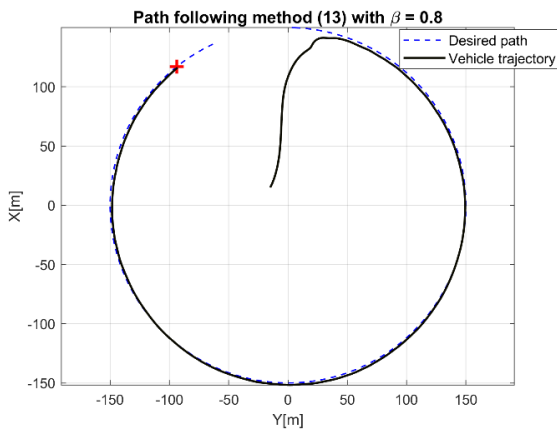
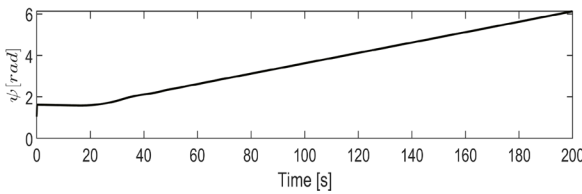b) Path tracking plotted for first 200 secs.

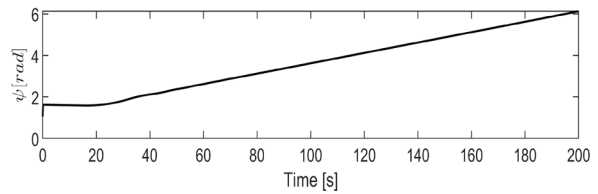(b) Surge and sway forces vs time

c) Components of $\boldsymbol{\tau}_c$ [N] in (13) with $\beta = 0.8$

(c) $\hat{\beta}(t)$ vs time

(d) Yaw angle vs time.

(d) Yaw angle vs time.

Fig. 2. Path following control under (13): (a) without and (b) with sliding mode control $\beta \mathrm{sign}(\mathbf{z})$.

Fig. 3. Path following control under adaptive controller (14) with $\hat{\beta}(0) = 0.05$, $k_\beta = 0.005$.

When an estimate of the upper bound of the disturbance, i.e., $\| \mathbf{w}_\mathbf{v} \|_\infty$, is unknown, path following control under adaptive controller (14) with $\hat{\beta}(0) = 0.05$ and $k_\beta = 0.005$ is reported in Fig. 3. It is shown that the vehicle tracks the desired path asymptotically and the update gain $\hat{\beta}(t)$ keeps increasing to slightly above 1 as time increases.

4.2. Path Following Control under Adaptive Controller (16)-(17)

We provide the simulation results for path following control of the vehicle under the continuous adaptive control laws (16)-(17) with $\hat{\beta}(0) = 0.05$, $k_{\beta} = 0.005$, and the normalizing signal being either $\mu(t) = e^{-0.05t}$ or $\mu(t) = e^{-0.005t}$ in Fig.4 and Fig. 5, respectively. Significant chattering reduction can be observed in the first two components of the control $\boldsymbol{\tau}_c$ (Fig. 4(b)) while path tracking performance is still comparable with that under adaptive controller (14). Note that the adaptive gain $\hat{\beta}(t)$ increases to roughly 0.74 and remains unchanged as time diverges, which

is less conservative than the adaptive gain under (14)-(15).

The control $\mathbf{u}_c$ can be made to vary significantly smooth using the normalizing signal $\mu(t) = e^{-0.005t}$, which diminishes slowly with time, as depicted in Fig.5 (b).

We further compare quantitatively the path tracking errors (8) of the controllers by computing the average and maximum position errors in the steady state (after 40 secs) as in Table 1. When there is no disturbance rejection term (controller (13) with $\beta = 0$) the position error is the highest among the controllers. The continuous tracking controller (16) with $\mu(t) = e^{-0.05t}$ achieves the lowest tracking error.
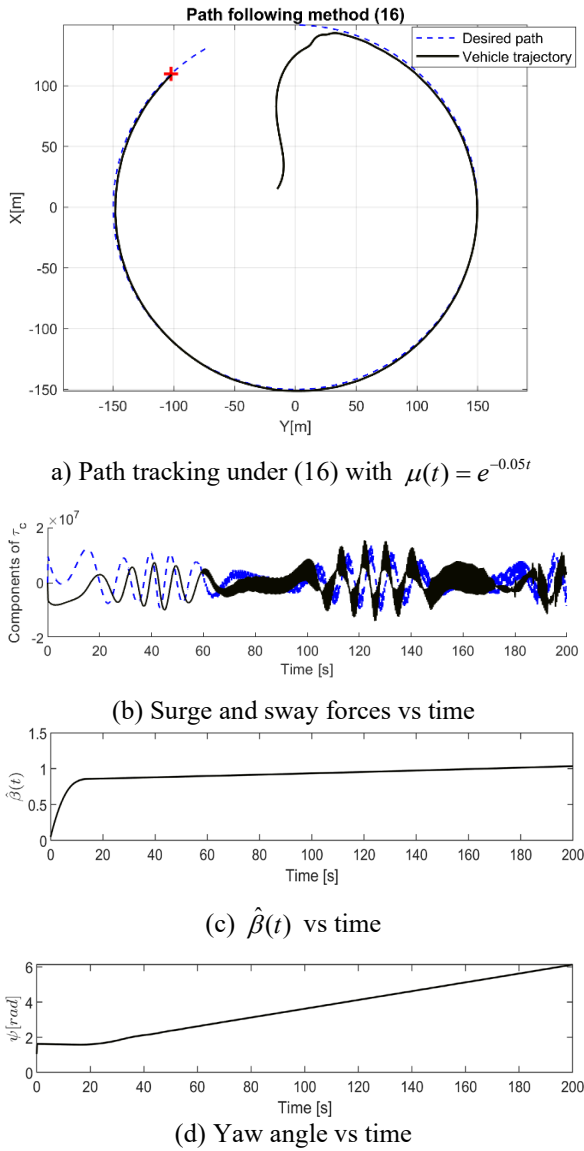

a) Path tracking under (16) with $\mu(t) = e^{-0.05t}$

(b) Surge and sway forces vs time

(c) $\hat{\beta}(t)$ vs time

(d) Yaw angle vs time

Fig. 4. Path following control under adaptive controller (16)-(17) with $\mu(t) = e^{-0.05t}$.

a) Path tracking under (16) with $\mu(t) = e^{-0.005t}$.

(b) Surge and sway forces vs time

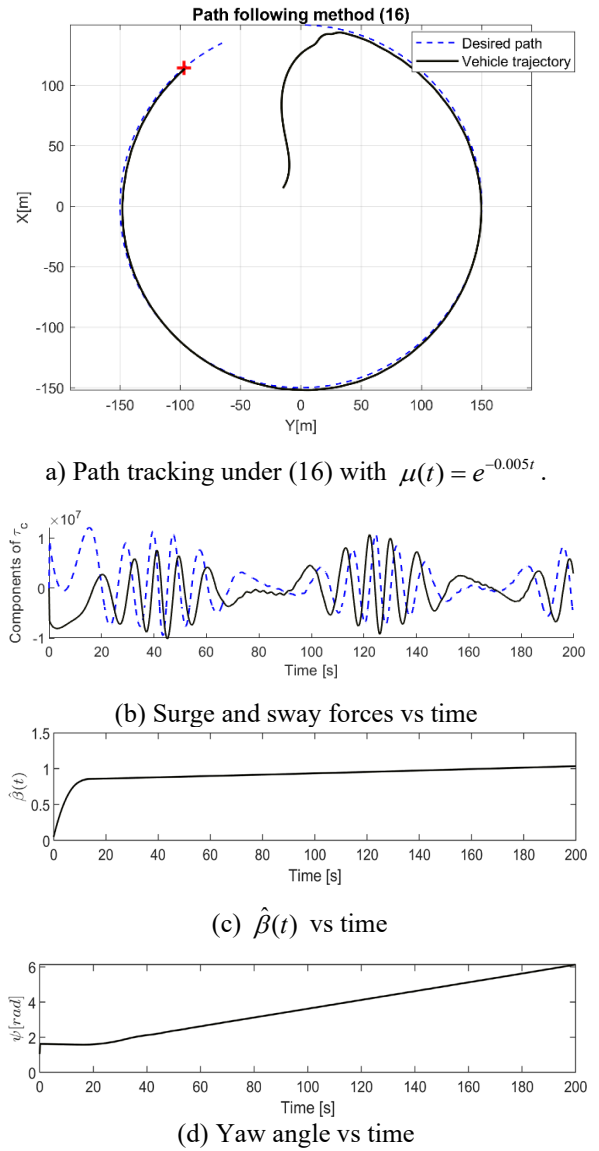(c) $\hat{\beta}(t)$ vs time

(d) Yaw angle vs time

Fig. 5. Path following control under adaptive controller (16)-(17) with $\mu(t) = e^{-0.005t}$.

Table 1. Comparison of the position error $\| \mathbf{e} \|=\| \mathbf{e}_{\mathcal{B}} \|=\| \mathbf{p}_d(\gamma)-\mathbf{p} \|$ in the steady state

Controllers	Mean error (m)	Max error (m)
(13) with $\beta = 0$	**3.07**	**5.46**
(13) with $\beta = 0.8$	1.82	2.98
(14) with $\hat{\beta}(0) = 0.05$	1.38	2.20
(16) with $\mu(t) = e^{-0.05t}$	1.3	2.17
(16) with $\mu(t) = e^{-0.005t}$	1.5	2.84

Note that the adaptive updates (15) and (17) are discretized with sampling time $T_s = 0.2$ sec while the dynamical vessel is a continuous time system. This discrepancy partly accounts for the position tracking errors. The position errors can also be made small by increasing the controllers' gains.

5. Conclusion

In this work, we have developed several robust path following control protocols for fully-actuated surface vehicles subject to unknown bounded disturbances. Adaptive control terms with time-varying control gains were utilized for path following with unknown disturbances. To overcome chattering effect in the control forces, a continuous path following controller based on a normalization method has been proposed. Under the proposed controllers, we established asymptotic convergence to the desired path of the vehicle based on Lyapunov stability theory and Barbalat's lemma. Simulation studies have demonstrated that the vehicle converges to desired path asymptotically. The position tracking error of the continuous tracking controller is the smallest among the controllers. Chattering can also be reduced significantly in the control forces of this continuous controller.

For future work, it is promising to extend the proposed adaptive controllers to the path following control of underactuated surface vehicles with only two independent actuators. Path following with obstacle avoidance based on Model Predictive Control (MPC) [5] or velocity obstacle methods [17] is also worthy of further investigation.

References

[1] Q. V. Tran, V. V. Nguyen, H. Q. Nguyen, Robust path following control of autonomous surface vessels, in Proc. ICCAS, Yeosu, Korea, Oct. 17-20, 2023, pp. 945–948.
https://doi.org/10.23919/ICCAS59377.2023.10316904

[2] A. P. Aguiar, J. A. P. Hespanha, Trajectory-tracking and path-following of underactuated autonomous vehicles with parametric modeling uncertainty, IEEE Transactions on Automatic Control, vol. 52, no. 8, pp. 1362–1379, 2007.
https://doi.org/10.1109/TAC.2007.902731

[3] L. Liu, D. Wang, Z. Peng, Path following of marine surface vehicles with dynamical uncertainty and time-varying ocean disturbances, Neurocomputing, vol. 173, pp. 799–808, Jan. 2016.
https://doi.org/10.1016/j.neucom.2015.08.033

[4] C. Lee, Q. V. Tran, and J. Kim, Robust path tracking and obstacle avoidance using tube-based model predictive control for surface vehicles, IFAC-PapersOnLine, vol. 55, no. 31, pp. 301–306, 2022.
https://doi.org/10.1016/j.ifacol.2022.10.446

[5] C. Lee, Q. V. Tran, J. Kim, Safety-guaranteed ship berthing using cascade tube-based model predictive control, IEEE Transactions on Control System Technology, vol. 32, no. 4, pp. 1504-1511, Jul. 2024.
https://doi.org/10.1109/TCST.2024.3374152

[6] Q. V. Tran et al., Robust bearing-based formation tracking control of underactuated surface vessels: An output regulation approach, IEEE Transactions on Control of Network Systems, vol. 10, no. 4, pp. 2048-2059, Dec. 2023.
https://doi.org/10.1109/TCNS.2023.3259105

[7] Caharija et al., Integral line-of-sight guidance and control of underactuated marine vehicles: Theory, simulations, and experiments, IEEE Transactions on Control Systems Technology, vol. 24, no. 5, pp. 1623-1642, Sep. 2016.
https://doi.org/10.1109/TCST.2015.2504838

[8] Su Y., Wan L., Zhang D., and Huang F., An improved adaptive integral line-of-sight guidance law for unmanned surface vehicles with uncertainties, Appl. Ocean Res, vol. 108, Mar. 2021, Art. no. 102488.
https://doi.org/10.1016/j.apor.2020.102488

[9] Fossen T. I., Pettersen K. Y., On uniform semiglobal exponential stability (USGES) of proportional line-of-sight guidance laws, Automatica, vol. 50, no.11, pp. 2912–2917, Nov. 2024.
https://doi.org/10.1016/j.automatica.2014.10.018

[10] H. Xu, C. G. Soares, Vector field path following for surface marine vessel and parameter identification based on LS-SVM. Ocean Eng., vol. 113, pp. 151–161, Feb. 2016.
https://doi.org/10.1016/j.oceaneng.2015.12.037

[11] Li M, Guo C, Yu H., Extended state observer-based integral line-of-sight guidance law for path following of underactuated unmanned surface vehicles with uncertainties and ocean currents, International Journal of Advanced Robotic Systems. vol.18(3), May. 2021.
https://doi.org/10.1177/17298814211011035

[12] Zhang H, Zhang X, Bu R, Sliding mode adaptive control for ship path following with sideslip angle observer, Ocean Eng, vol. 251, May. 2022, Art. no. 111106.

https://doi.org/10.1016/j.oceaneng.2022.111106

[13] Zhang G, Han J, Li J, Zhang X, APF-based intelligent navigation approach for USV in presence of mixed potential directions: Guidance and control design. Ocean Eng, vol. 260, Sep. 2022, Art. no. 111972. https://doi.org/10.1016/j.oceaneng.2022.111972

[14] T. I. Fossen, Handbook of Marine Craft Hydrodynamics and Motion Control, John Wiley & Sons, 2011. https://doi.org/10.1002/9781119994138

[15] D. Shevitz, B. Paden, Lyapunov stability theory of nonsmooth systems, IEEE Transactions on Automatic Control, vol. 39, no. 9, pp. 1910–1914, Sep. 1994. https://doi.org/10.1109/9.317122

[16] P. A. Ioannou and J. Sun, Robust Adaptive Control, Courier Corporation, 2012.

[17] A. Haraldsen, M. S. Wiig, K. Y. Pettersen, A theoretical analysis of the velocity obstacle method for nonholonomic vehicles and underactuated surface vessels, IEEE Transactions on Control Systems Technology (Early Access), pp. 1-16, Mar. 2024. https://doi.org/10.1109/TCST.2024.3375023